Phys. Scr. **86** (2012) 045302 (6pp) doi:10.1088/0031-8949/86/04/045302

Autoionization widths of open-M-shell germanium ions: effects on inner-shell absorptions

Wenjun Xiang, Yongsheng Fu, Cheng Gao and Jiaolong Zeng

Department of Physics, College of Science, National University of Defense Technology, Changsha Hunan 410073, People's Republic of China

E-mail: jlzeng@nudt.edu.cn

Received 11 March 2012
Accepted for publication 29 August 2012
Published 27 September 2012
Online at stacks.iop.org/PhysScr/86/045302

Abstract

Large-scale configuration interaction calculations were carried out to obtain the level-by-level autoionization (AI) rates and resonance widths of the inner-shell excited configurations for the open-M-shell germanium ions. Detailed results are presented for Ge^{5+} as an example. The dominant ionization channels of the autoionized levels $2p^5_{3/2}3s^23p^63d^{10}$ and $2p^5_{1/2}3s^23p^63d^{10}$ of Ge^{5+} were determined, and it is shown that the channel from level $3s^23p^6(3d^{-1}_{3/2}3d^{-1}_{5/2})_4$ contributes the largest fraction of AI widths of 0.195 and 0.188 eV to the total width of 0.577 and 0.544 eV, respectively, from all possible channels. For typical experimental plasmas at temperatures of several tens and hundreds of eV, the AI resonance broadening is the dominant mechanism among the Doppler, electron impact and natural lifetime broadenings. Among the physical effects such as relativistic and the interaction between fine-structure levels belonging to the same non-relativistic configuration and different configurations, particular attention is paid to the effect of AI resonance broadening on the L-shell absorption. Different features of the inner-shell absorption due to AI broadening are presented in detail for Ge^{5+}, Ge^{10+} and Ge^{17+}. The total AI widths of levels from the configuration of one 2p electron being excited to 3d orbital were systematically investigated for Ge^{6+}–Ge^{21+}. Except for Ge^{20+} and Ge^{21+}, the AI widths of the open-M-shell germanium ions dominate over all other line broadening mechanisms.

PACS numbers: 32.80.Zb, 32.70.Jz, 32.30.Rj

1. Introduction

Germanium is one of the materials used for x-ray pre-heat shielding in indirectly driven inertial confinement fusion and therefore its radiative property is of great interest both experimentally and theoretically [1–9]. The radiative opacity of open-M-shell germanium plasmas is of particular experimental interest, especially in the region of 2p–3d transition arrays. Foster *et al* [1] measured the L-shell absorption spectrum of a germanium plasma, which was generated by radiation heating using thermal × radiation from a laser-produced gold plasma. Tracer elements of Al and Mg were used to characterize the temperature (76 eV) and density (0.05 g cm^{-3}) of the plasma. Perry *et al* [2] experimentally measured the x-ray absorption of germanium plasmas at a lower temperature of about 38 eV. Renaudin *et al* [3] measured the absorption spectra of germanium plasma in the 0.8–1.1 nm range. The germanium sample was radiatively heated by a gold hohlraum. Recently, Loisel *et al* [4] experimentally measured the radiative opacity of medium Z element plasmas including germanium in the x-ray region (0.8–1.8 nm) at temperatures between 15 and 25 eV and densities between 2 and 10 mg cm^{-3}.

The wide interest in experimental and theoretical work on the L-shell absorptions of germanium plasmas is partly due to the strong emission or absorption in this photon energy region, which is useful for indirectly driven inertial confinement fusion. On the other hand, the 2p–3d absorption lines are ideal tools for the diagnostics of the physical condition of experimental plasmas. Therefore, accurate determination of

the main line broadening mechanisms is very important for the diagnostics of physical conditions such as the plasma temperature and density. In a recent work, Blenski *et al* [10] carried out a theoretical interpretation of the x-ray photo-absorption experiments measured at the LULI2000 facility [4]. Their analysis was performed using the statistical superconfiguration code SCO, two line-by-line opacity codes based on the HULLAC and Flexible Atomic Code (FAC) packages and a hybrid statistical-detailed code, SCORCG. The authors pointed out that in the detailed line-by-line treatment, autoionization (AI) resonance broadening appeared to be the most important of all broadening mechanisms. However, no detailed investigations were found in the literature on this effect partly due to the highly challenging computations of the detailed line spectrum with the complex open-M-shell germanium ions.

In this work, we investigated the inner-shell AI rates and widths of the open-M-shell germanium ions, which should be useful for the accurate calculation of the x-ray radiative opacity of Ge plasmas. To gain a better understanding of the relative importance of various line broadening mechanisms, comparisons are made with the lifetime, Doppler and electron impact broadenings. To the best of our knowledge, no detailed investigations on the inner-shell excited AI rates and widths of the open-M-shell germanium ions are found in the literature. More than 20 years ago, Ryabtsev and Wyart [11] carried out research on valence excited AI energy levels and spectral analysis of copper-like germanium (Ge IV). Accurate AI rates are also important to determine the population balance and radiative properties in non-local thermodynamic equilibrium (non-LTE) plasmas with a wide range of temperatures and densities [12–18].

2. Theoretical method

The calculations have been carried out using the FAC developed by Gu [19]. A fully relativistic approach based on the Dirac equation was used throughout the entire package. An atomic state is approximated by a linear combination of configuration state functions (CSFs) with same symmetry

$$\Phi_\alpha(J\pi) = \sum_i^{n_c} a_i(\alpha)\phi_\alpha(J\pi), \tag{1}$$

where n_c is the number of CSFs and $a_i(\alpha)$ denotes the representation of the atomic state in this basis. The CSFs are anti-symmetrized products of a common set of orthogonal orbitals which are optimized on the basis of the relativistic Hamiltonian. The radial orbitals are derived from a modified Dirac–Fock–Slater iteration on a fictitious mean configuration with fractional occupation numbers, representing the average electron cloud of the configurations included in the calculation.

The AI rates are obtained in the relativistic distorted-wave approximation. In the first-order perturbation theory, the AI rate can be written as (in atomic units)

$$A^{\mathrm{a}}_{ij} = \sum_\kappa |\langle\psi_j, \kappa;\, J_{\mathrm{T}} M_{\mathrm{T}}| \sum_{i<j} \frac{1}{r_{ij}} |\psi_i\rangle|^2, \tag{2}$$

where ψ_i is the autoionzing state, ψ_j is the final state which has one electron less than ψ_i and κ is the relativistic angular quantum number of the free electron. The total angular quantum number of the coupled final state must be equal to that of ψ_i, i.e. $J_{\mathrm{T}} = J_i$ and $M_{\mathrm{T}} = M_i$. For a particular autoionizing level, there are many AI channels. The full-width at half-maximum (FWHM) due to the AI resonance broadening can be obtained by summing up all possible channels

$$\Gamma^{\mathrm{a}}_i = \hbar \sum_j A^{\mathrm{a}}_{ij}, \tag{3}$$

where $\hbar = h/2\pi$ and h is the Planck constant. To obtain accurate atomic data, one should include adequate configuration interaction in both autoionized and recombined ions.

3. Results and discussion

We systematically investigated the AI rates and widths of germanium ions ranging from Ge^{5+} (the ground configuration $[Ne]3s^23p^63d^9$) to Ge^{21+} (the ground configuration [Ne]3s). These charge states have a complex atomic structure with open-M-shell characteristics, and it is a challenging task to accurately determine their atomic data including AI rates and widths. Under the experimental conditions mentioned above [1–4], the charge states that contribute to the L-shell absorption fall into these ion types.

Ge^{5+} is the lowest ionization stage which has L-shell absorptions of 2p–3d transitions, where there are two levels for the inner-shell 2p excited configuration $2p^53s^23p^63d^{10}$ (which is labelled as $2p^{-1}_{3/2}$ and $2p^{-1}_{1/2}$, respectively, with the full orbitals being omitted for simplicity). Table 1 gives the AI rates of the main channels from these two levels with the AI rate being larger than $1.0 \times 10^{13}\,\mathrm{s}^{-1}$. Note that $3d^{-1}_{3/2}$ and $3d^{-1}_{5/2}$ denote a hole in the relativistic orbitals of $3d_{3/2}$ and $3d_{5/2}$. To obtain the results, the interaction between the following configurations was included in the calculations: $2p^63s^23p^63d^9$, $2p^63s^23p^63d^8nl$, $2p^63s^23p^53d^{10}$, $2p^63s^23p^53d^9nl$, $2p^53s^23p^63d^{10}$, $2p^53s^23p^63d^9nl$ $(n = 4, 5, 6, l = 0, 1, 2, \ldots, n-1)$ for Ge^{5+}, $2p^63s^23p^63d^8$, $2p^63s^23p^63d^7nl$, $2p^63s^23p^53d^9$, $2p^63s^23p^53d^8nl$, $2p^63s3p^63d^9$, $2p^63s^23p^53d^8nl$ $(n = 4, 5, 6, l = 0, 1, 2, \ldots, n-1)$ for Ge^{6+}.

From the inspection of table 1, one can see that the dominant ionization channels of the levels $2p^{-1}_{3/2}$ and $2p^{-1}_{1/2}$ from configuration $2p^53s^23p^63d^{10}$ originate from levels of $2p^63s^23p^63d^8$ and $2p^63s^23p^53d^9$ configurations, while levels of other configurations such as $2p^63s^23p^63d^74d$, $2p^63s^23p^63d^74f$ and $2p^63s^23p^63d^75s$ have definite contributions. For both $2p^{-1}_{3/2}$ and $2p^{-1}_{1/2}$ autoionized levels, the channel from level $(3d^{-1}_{3/2}3d^{-1}_{5/2})_4$ contributes the largest AI width of 0.195 and 0.188 eV, respectively. The second largest AI channel originates from $(3p^{-1}_{1/2}3d^{-1}_{5/2})_3$, with the width being 0.094 and 0.105 eV, respectively. The last column lists the contribution to the AI widths from the respective AI channels. By summing up the partial contributions from all the channels, one can determine the total AI resonance width of $2p^{-1}_{3/2}$ and $2p^{-1}_{1/2}$ levels to be 0.577 and 0.544 eV, respectively.

Table 1. AI rates and widths of Ge VI from energy levels belonging to the excited configuration $2p^5 3s^2 3p^6 3d^{10}$ to the final energy levels, where only rates larger than 1.0×10^{13} s^{-1} are given. Note that full subshells are omitted for simplicity.

AI level	AI channel	J	ΔE (eV)	AI rate (10^{13} s^{-1})	AI width (eV)
$2p_{3/2}^{-1}$	$3d_{5/2}^{-2}$	4	1077.8	5.746	0.0378
$2p_{3/2}^{-1}$	$3d_{3/2}^{-1}3d_{5/2}^{-1}$	3	1077.4	3.563	0.0235
$2p_{3/2}^{-1}$	$3d_{3/2}^{-2}$	2	1077.2	2.710	0.0178
$2p_{3/2}^{-1}$	$3d_{5/2}^{-2}$	2	1074.8	4.199	0.0276
$2p_{3/2}^{-1}$	$3d_{3/2}^{-1}3d_{5/2}^{-1}$	2	1074.0	1.044	0.0069
$2p_{3/2}^{-1}$	$3d_{3/2}^{-1}3d_{5/2}^{-1}$	4	1072.9	29.66	0.1952
$2p_{3/2}^{-1}$	$3p_{3/2}^{-1}3d_{3/2}^{-1}$	1	977.15	1.792	0.0118
$2p_{3/2}^{-1}$	$3p_{3/2}^{-1}3d_{3/2}^{-1}$	2	976.52	3.371	0.0222
$2p_{3/2}^{-1}$	$3p_{3/2}^{-1}3d_{5/2}^{-1}$	3	975.95	6.328	0.0416
$2p_{3/2}^{-1}$	$3p_{3/2}^{-1}3d_{5/2}^{-1}$	1	974.57	2.352	0.0155
$2p_{3/2}^{-1}$	$3p_{1/2}^{-1}3d_{5/2}^{-1}$	2	973.57	1.199	0.0079
$2p_{3/2}^{-1}$	$3p_{1/2}^{-1}3d_{3/2}^{-1}$	1	966.08	3.416	0.0225
$2p_{3/2}^{-1}$	$3p_{1/2}^{-1}3d_{5/2}^{-1}$	3	965.18	14.23	0.0937
$2p_{3/2}^{-1}$	$(3d_{3/2}^{-2}3d_{5/2}^{-1})_{9/2}4f_{5/2}$	3	957.39	1.177	0.0077
$2p_{1/2}^{-1}$	$3d_{5/2}^{-2}$	4	1108.9	2.548	0.0168
$2p_{1/2}^{-1}$	$3d_{3/2}^{-1}3d_{5/2}^{-1}$	3	1108.5	3.658	0.0241
$2p_{1/2}^{-1}$	$3d_{3/2}^{-2}$	2	1108.2	2.423	0.0159
$2p_{1/2}^{-1}$	$3d_{5/2}^{-2}$	2	1105.9	4.667	0.0307
$2p_{1/2}^{-1}$	$3d_{3/2}^{-1}3d_{5/2}^{-1}$	2	1105.1	1.214	0.0080
$2p_{1/2}^{-1}$	$3d_{3/2}^{-1}3d_{5/2}^{-1}$	4	1104.0	28.51	0.1877
$2p_{1/2}^{-1}$	$3p_{3/2}^{-1}3d_{5/2}^{-1}$	3	1007.0	1.626	0.0107
$2p_{1/2}^{-1}$	$3p_{3/2}^{-1}3d_{5/2}^{-1}$	1	1005.7	1.639	0.0108
$2p_{1/2}^{-1}$	$3p_{1/2}^{-1}3d_{5/2}^{-1}$	2	1004.7	5.782	0.0381
$2p_{1/2}^{-1}$	$3p_{1/2}^{-1}3d_{3/2}^{-1}$	1	997.16	6.399	0.0421
$2p_{1/2}^{-1}$	$3p_{1/2}^{-1}3d_{5/2}^{-1}$	3	996.26	15.98	0.1052
$2p_{1/2}^{-1}$	$(3d_{3/2}^{-2}3d_{5/2}^{-1})_{9/2}4f_{5/2}$	3	988.48	1.302	0.0086

Table 2. The transition energy ΔE, weighted oscillator strengths and natural lifetime width Γ_n for an inner-shell transition array of $2p^6 3s^2 3p^6 3d^9$–$2p^5 3s^2 3p^6 3d^{10}$.

Transition	ΔE (eV)	gf	Γ_n (meV)
$2p_{3/2}^{-1}$–$3d_{5/2}$	1179.9	1.026	5.8
$2p_{3/2}^{-1}$–$3d_{3/2}$	1179.3	0.115	5.8
$2p_{1/2}^{-1}$–$3d_{3/2}$	1210.4	0.552	5.9

We first compare the AI width with the natural lifetime width of the inner-shell transitions from 2p electrons. The AI resonance width of $2p_{3/2}^{-1}$ and $2p_{1/2}^{-1}$ levels is by far larger than the line width of the natural lifetime. Table 2 lists the transition energy, weighted oscillator strengths and natural lifetime widths for the transition array of $2p^6 3s^2 3p^6 3d^9$–$2p^5 3s^2 3p^6 3d^{10}$. The oscillator strengths are obtained in the same theoretical formalism as in the calculations of AI rates. Using the same set of the CSFs constructed in calculations of AI rates, the weighted oscillator strengths can be calculated as

$$g_i f_{ij} = \frac{2\Delta E}{3}(|\langle \Phi_i \,|\vec{\mathbf{P}}|\, \Phi_j \rangle|)^2, \qquad (4)$$

where $\Delta E = E_j - E_i$, E_i and E_j are, respectively, the energies of the initial and final levels and g_i is the statistical weight of the lower level, i.e. $g_i = 2J_i + 1$, and J_i is the total angular momentum of the lower level. $\vec{\mathbf{P}}$ is a dipole transition operator with $\vec{\mathbf{P}} = \sum_{p=1}^{N} \vec{\mathbf{r}}_p$ in the length formalism and $\vec{\mathbf{P}} = \frac{2}{\Delta E}\sum_{p=1}^{N} \vec{\nabla}_p$ in the velocity formalism, where N is the total number of bound electrons. By using the same method as that used in obtaining the AI resonance width, we can determine the natural lifetime width for the three transitions to be 5.8, 5.8 and 5.9 meV (1 meV = 0.001 eV), which is much smaller than the corresponding AI resonance width of 0.577 and 0.544 eV.

For the 2p–3d transition array of Ge^{5+}, there are three dipole-allowed fine-structure transitions: $2p_{3/2}$–$3d_{5/2}$, $2p_{1/2}$–$3d_{3/2}$ and $2p_{3/2}$–$3d_{3/2}$. The radiative transition probability of the last transition is much smaller than the first two lines. The effect of AI resonance width on the absorption in the 2p–3d region can be clearly seen from figure 1, which shows the absorption cross section for the transition array of $2p^6 3s^2 3p^6 3d^9$–$2p^5 3s^2 3p^6 3d^{10}$ of Ge^{5+}. In order to obtain the results, Ge^{5+} was assumed to be embedded in an LTE plasma at a temperature of 16 eV and a density of 0.01 g cm^{-3}. In figure 1(b), the natural lifetime, electron impact and Doppler broadening mechanisms were taken into account, while the AI

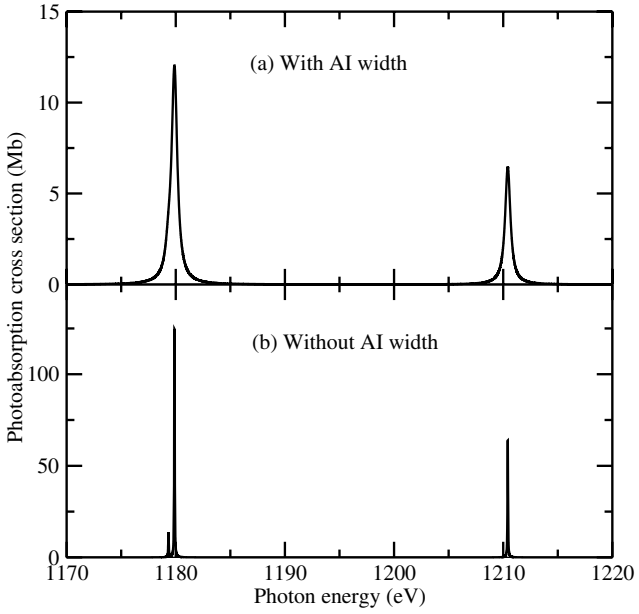

Figure 1. Absorption cross section for the transition array of $2p^63s^23p^63d^9$–$2p^53s^23p^63d^{10}$ of Ge^{5+}: (a) including and (b) not including the effect of AI resonance broadening.

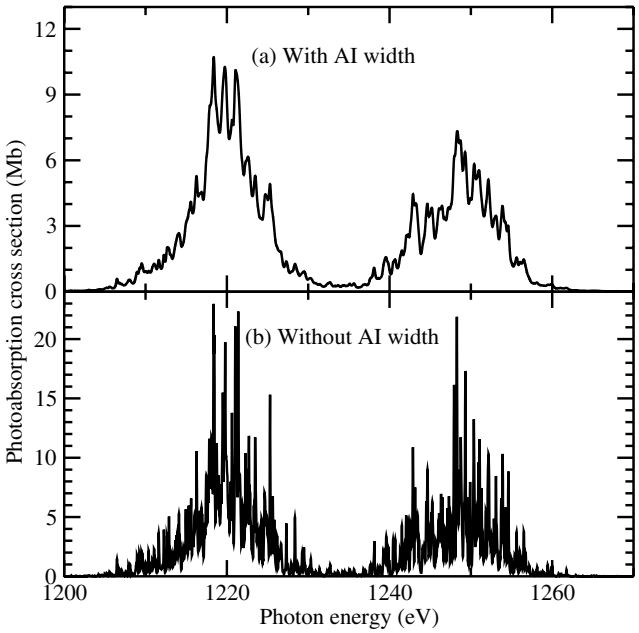

Figure 2. The same as figure 1 but for the transition array of $2p^63s^23p^63d^4$–$2p^53s^23p^63d^5$ of Ge^{10+}.

resonance broadening is not included. In figure 1(a), further AI resonance broadenings were also taken into account. The FWHM due to the Doppler broadening Γ_d is related to the temperature T of the plasma and transition energy ΔE [20]

$$\Gamma_d = 7.716 \times 10^{-5}(kT/A)^{1/2}\Delta E, \tag{5}$$

where A is the atomic weight of the ion in grams, and the units of kT, ΔE and Γ_d are eV. For the FWHM of electron impact broadening, we use a semi-empirical method [21, 22]

$$\Gamma_e = N_e \frac{8\pi}{6}\frac{\hbar^3}{m^2 e}\left(\frac{2m}{\pi kT}\right)^{1/2}\frac{\pi}{\sqrt{3}}\left(0.9-\frac{1.1}{z}\right) \times \sum_{j=i,f}\left(\frac{3n_j}{2z}\right)^2 (n_j^2 - l_j^2 - l_j - 1), \tag{6}$$

where n_i (l_i) and n_f (l_f) are the effective principal (orbital angular momentum) quantum numbers of the lower and upper energy levels of the transition, respectively.

The effect of AI resonance broadening on the absorption of Ge^{5+} is evident from the inspection of figure 1. Note that a different scale has been used in figures 1(a) and (b) to have a clear demonstration of the results. A Voigt profile was utilized with the natural lifetime, electron impact and AI resonance broadening as the Lorentzian components and Doppler broadening as the Gaussian component. One can see that when AI resonance broadening is included, the peak absorption cross section is more than one order of magnitude smaller, which is a reflection of the effect of AI resonance broadening on absorption. In the above plasma conditions, the FWHM due to electron impact and Doppler broadening is evaluated to be 0.028 and 0.044 eV, respectively. The FWHM due to AI resonance broadening is 0.577 and 0.544 eV for 2p excited levels of $2p_{3/2}^{-1}$ and $2p_{1/2}^{-1}$, respectively. Among all the broadening mechanisms, the AI resonance broadening is the most important. It is larger than the natural lifetime, electron impact and Doppler width by more than one order of magnitude.

As there are only two strong absorption lines for Ge^{5+} and as the 2p–3d spin–orbit splitting (30 eV) is much larger than the line width caused by all broadening mechanisms, two 2p–3d transition lines are separate from each other with an interval of 30 eV. With a decrease of the number of 3d electrons, especially near the half full 3d orbital, the number of 2p–3d lines rapidly increases and the absorption approaches unresolved quasi-continuum bands. Figure 2 shows the absorption cross section for the transition array of $2p^63s^23p^63d^4$–$2p^53s^23p^63d^5$ of Ge^{10+}, which was assumed to be embedded in an LTE plasma at a temperature of 38 eV and a density of 0.015 g cm^{-3}. Similar to Ge^{5+}, the AI resonance width is also larger than the natural lifetime, electron impact and Doppler width by more than one order of magnitude. However, the peak absorption cross section without considering the AI resonance broadening is just 1.35 times larger than that which includes this effect. This is due to many lines overlapping together, resulting in less pronounced effects than those in Ge^{5+}, where lines do not overlap. The two strong absorption bands with an interval of spin–orbit splitting of 30 eV in figure 2 originate from the relativistic splitting of $2p_{3/2}$–$3d_{5/2}$ and $2p_{1/2}$–$3d_{3/2}$ transitions for the lower and higher photon energy ranges, respectively. Such a feature differs obviously from that of Ge^{5+}.

With a further increase of the ionization stage, the 2p–3d absorption shows a different feature than Ge^{5+} and Ge^{10+}, as illustrated in figure 3, which shows the absorption cross section for the transition array of $2p^63s^23p^3$–$2p^53s^23p^33d$ of Ge^{17+}. Ge^{17+} was assumed to be embedded in an LTE plasma at a temperature of 90 eV and a density of 0.015 g cm^{-3}. For Ge^{5+} and Ge^{10+}, the $2p_{3/2}$–$3d_{5/2}$ absorption is stronger than $2p_{1/2}$–$3d_{3/2}$, while this is reversed for Ge^{17+}. The peak absorption cross section changes from locating at 1332 eV (one of $2p_{1/2}$–$3d_{3/2}$ transitions) without including the AI width to 1293 eV (one of $2p_{3/2}$–$3d_{5/2}$ transitions) with

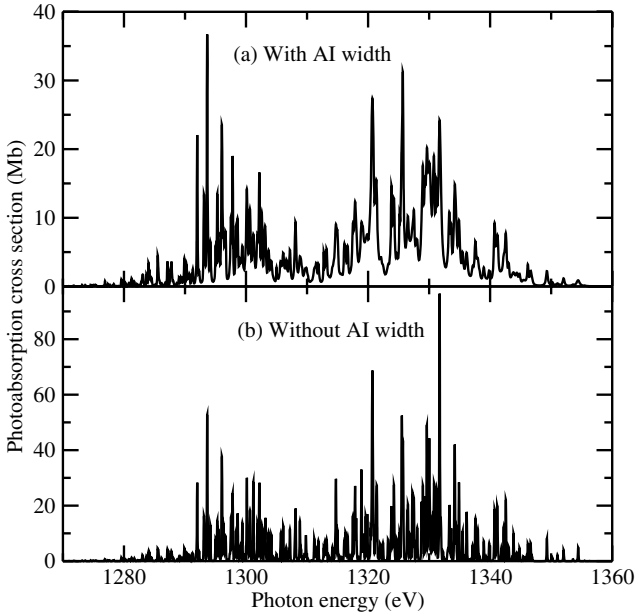

Figure 3. The same as figure 1 but for the transition array of $2p^63s^23p^3$–$2p^53s^23p^33d$ of Ge^{17+}.

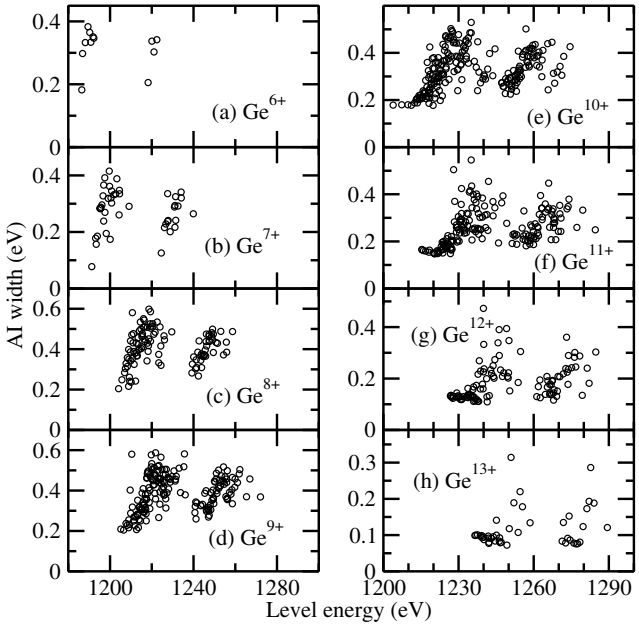

Figure 4. AI width of the levels from the 2p–3d excited configuration of Ge^{6}+–Ge^{13+}.

including AI. Furthermore, the results show that the AI width for many upper levels of $2p_{3/2}$–$3d_{5/2}$ transitions is smaller than many of $2p_{1/2}$–$3d_{3/2}$.

To gain an overall understanding of the AI resonance width for Ge^{5+}–Ge^{21+}, we show the AI width of the levels of inner-shell excited configuration with one 2p electron being excited to 3d in figure 4 for Ge^{6+}–Ge^{13+} and figure 5 for Ge^{14+}–Ge^{21+}, with the abscissa denoting the relative energy of levels to the respective ground level. It can be seen that the AI width of the inner-shell excited levels of Ge^{6+}–Ge^{19+} scattered in the region of 0.01–0.7 eV, while that of Ge^{20+} and Ge^{21+} is smaller than 0.01 eV, which is much smaller than lower ionization stages. For Ge^{6+}–Ge^{9+} ions, all 2p

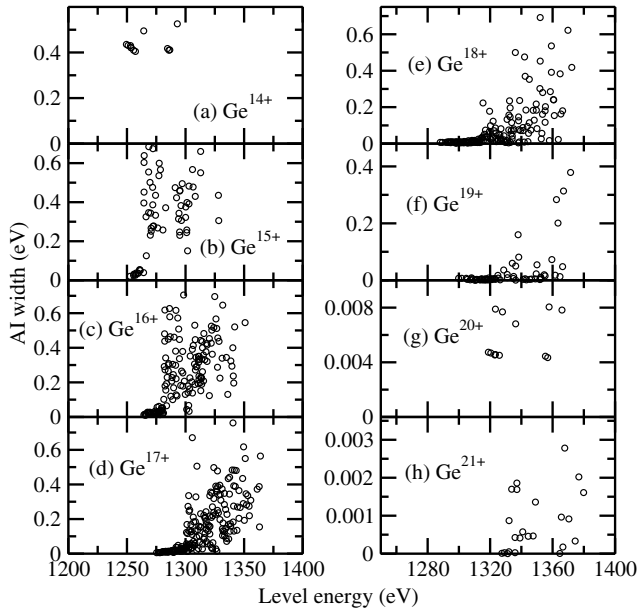

Figure 5. AI width of the levels from the 2p–3d excited configuration of Ge^{14+}–Ge^{21+}.

excited levels have a strong tendency to autoionize with the minimal AI resonance width being about 0.2 eV. The minimal AI width gradually decreases to 0.1 eV for Ge^{10+}–Ge^{13+}. The ions of Ge^{6+}–Ge^{13+} have open 3d shell ground electronic configuration $3s^23p^63d^n$ with $n = 8$ for Ge^{6+} and $n = 1$ for Ge^{13+}. For Ge^{14+}, with the ground configuration of $3s^23p^6$, the AI width ranges from 0.4 to 0.53 eV for the levels of 2p excited configuration of $2p^53s^23p^63d$. For ions with open 3p electronic configuration $3s^23p^n$ from Ge^{15+} ($n = 5$) to Ge^{19+} ($n = 1$), the maximal AI width exceeds 0.6 eV except for Ge^{19+}, while the minimal width tends to be very small (~ 0.01 eV). With an increase of the ionization stage from Ge^{15+} to Ge^{19+}, more and more levels have a small AI width of less than 0.1 eV. For Ge^{15+} and Ge^{16+}, the AI width of most of the 2p excited levels is larger than 0.1 eV and therefore have a strong tendency to autoionize. For Ge^{17+}, however, only about half of the inner-shell excited levels have a width larger than 0.1 eV. Concerning higher charge states of Ge^{18+} and Ge^{19+}, it is completely contrary to the case of Ge^{15+} and Ge^{16+} with most levels having a small width of less than 0.1 eV. For Ge^{20+} (ground configuration ([Ne])$3s^2$) and Ge^{21+} (ground configuration ([Ne])3s), the AI width tends to be smaller than 0.01 eV, which is, however, a little smaller than the Doppler width for typical plasma conditions with a temperature of 100–300 eV. For these two ions, AI resonance broadening is not the dominant mechanism.

In conclusion, systematic investigations were carried out for the AI rates and resonance widths of the inner-shell 2p excited fine-structure levels for the open-M-shell germanium ions from Ge^{5+} to Ge^{21+} by using large-scale configuration interaction calculations. For Ge^{5+}, the two most important AI channels of the autoionized levels $2p^5_{3/2}3s^23p^63d^{10}$ and $2p^5_{1/2}3s^23p^63d^{10}$ were contributed from levels $(3d^{-1}_{3/2}3d^{-1}_{5/2})_4$ and $(3p^{-1}_{1/2}3d^{-1}_{5/2})_3$, accounting for the half contribution of the total width of 0.577 and 0.544 eV, respectively. For typical experimental plasmas at temperatures of several tens to a few hundreds of eV, the AI resonance broadening is the

dominant mechanism among the Doppler, electron impact and natural lifetime broadenings for the open-M-shell germanium ions Ge^{5+}–Ge^{19+} except for Ge^{20+} and Ge^{21+}. The effects of AI resonance broadening on the L-shell absorption were presented in detail for Ge^{5+}, Ge^{10+} and Ge^{17+} as examples. Such effects are most pronounced for nearly full-filled 3d or 3p subshell germanium ions such as Ge^{5+} with just a few 2p–3d transition lines, while it is less pronounced for nearly half-filled 3d or 3p complex ions such as Ge^{10+} and Ge^{17+}, where there are so many 2p–3d lines whose line overlapping partly conceals the effect of AI resonance broadening. The abnormality happens in Ge^{20+} and Ge^{21+}, where the AI resonance broadening is not the main broadening mechanism. The present study should be useful for the diagnosis of the plasma temperature by using 2p–3d inner-shell absorption.

Acknowledgments

This work was supported by the National Natural Science Foundation of China under grant no. 11274382.

References

[1] Foster J M, Hoarty D J, Smith C C, Rosen P A, Davidson S J, Rose S J, Perry T S and Serduke F J D 1991 *Phys. Rev. Lett.* **67** 3255
[2] Perry T S *et al* 1995 *J. Quantum Spectrosc. Radiat. Transfer* **54** 317
[3] Renaudin P, Blancard C, Bruneau J, Faussurier G, Fuchs J-E and Gary S 2006 *J. Quantum Spectrosc. Radiat. Transfer* **99** 511
[4] Loisel G *et al* 2009 *High Energy Density Phys.* **5** 173
[5] Hoarty D J, James S F, Brown C R D, Williams B M, Chung H K, Harris J W O, Upcraft L M, Crowley B J B, Smith C C and Lee R W 2010 *High Energy Density Phys.* **6** 105
[6] Harris J W O, Upcraft L M, Hoarty D J, Crowley B J B, Brown C R D and James S F 2010 *High Energy Density Phys.* **6** 95
[7] Peng Y L, Xia D and Li J M 2004 *J. Quantum Spectrosc. Radiat. Transfer* **87** 95
[8] White V J L, Foster J M, Hansom J C V and Rosen P A 1994 *Phys. Rev.* E **49** R4803
[9] Jun Y and Jiaming L 2000 *Chin. Phys. Lett.* **17** 194
[10] Blenski T *et al* 2010 *High Energy Density Phys.* **7** 320
[11] Ryabtsev A N and Wyart J-F 1987 *Phys. Scr.* **36** 255
[12] Fontes C J, Abdallah J Jr, Bowen C, Lee R W and Ralchenko Y 2009 *High Energy Density Phys.* **5** 15
[13] Albritton J R and Wilson B G 1999 *Phys. Rev. Lett.* **83** 1594
[14] Hahn Y 1997 *Rep. Prog. Phys.* **60** 691
[15] Jacobs V L 1995 *J. Quantum Spectrosc. Radiat. Transfer* **54** 195
[16] Bauche J, Bauche-Arnoult C and Peyrusse O 2009 *High Energy Density Phys.* **5** 51
[17] Jacobs V L 2009 *High Energy Density Phys.* **5** 80
[18] Gao C and Zeng J 2010 *Phys. Rev.* A **82** 062515
[19] Gu M F 2003 *Astrophys. J.* **582** 1241
[20] Cowan R D 1981 *Theory of Atomic Spectra* (Berkeley, CA: University of California Press)
[21] Dimitrijevic M S and Konjevic N 1980 *J. Quantum Spectrosc. Radiat. Transfer* **24** 451
[22] Dimitrijevic M S and Konjevic N 1987 *Astron. Astrophys.* **172** 345